Nanoparticle-Induced Controlled Biodegradation and Its Mechanism in Poly(ε-caprolactone)

Narendra K. Singh,[†] Biswapratim Das Purkayastha,[‡] Jagat K. Roy,[‡] Rathindra M. Banik,[§] Madhu Yashpal,[∥] Gajendra Singh,[∥] Sudip Malik,[⊥] and Pralay Maiti*[,†]

School of Materials Science and Technology and School of Biochemical Engineering, Institute of Technology, Department of Zoology, and Anatomy Department, Institute of Medical Science, Banaras Hindu University, Varanasi 221 005, India, and Polymer Science Unit, Indian Association for the Cultivation of Science, Jadavpur, Kolkata 700 032, India

ABSTRACT Poly(ε-caprolactone) (PCL)/layered silicate nanocomposites have been prepared via solution route. Two different organically modified nanoclays were used to compare the variation in properties based on organic modifications. The nanostructures, as observed from wide-angle X-ray diffraction and transmission electron microscopy, indicate intercalated and partially exfoliated hybrids depending on the nature of organic modification in nanoclay. The nanohybrids exhibit significant improvement in thermal and mechanical properties of the matrix as compared to neat polymer. The nanoclays act as nucleating agent for the crystallization of PCL. The biodegradability of pure PCL and its nanocomposites have been studied under controlled conditions in enzyme, pure microorganism (fungi), compost, Ganges water, and alkaline buffer solution. The rate of biodegradation of PCL has enhanced dramatically in nanohybrids and depends strongly on the media used. Scanning confocal, electron, and atomic force microscopes have used to demarcate the nature of biodegradation of pristine PCL and its nanocomposites. The change in biodegradation is rationalized in terms of the crystallization behavior and organic modification in nanoclays of the nanohybrids vis-à-vis the neat polymer. The extent of compatibility was measured quantitatively through the interaction parameter for two different nanoclays to compare and establish the reason for variation in their properties in nanohybrids. A biodegradation mechanism has been revealed for PCL and its nanocomposites through enzyme activity in varying pH environment.

KEYWORDS: poly(ε-caprolactone) • nanocomposites • biodegradation • morphology and nanostructure

INTRODUCTION

The recycling of commodity plastics is limited; most are irrecoverable and end up in landfill burial sites for thousands of years, as they are nonbiodegradable in nature. There are many environmental problems associated with the method of disposal of plastic waste causing shortage of landfill space, emissions during incineration, and negative impact on wildlife through ingestion and entrapment, which stimulated interest in developing biodegradable plastics. Polymer based on polyhydroxyalkanoates, synthesized from microorganisms, are biodegradable but very expensive to produce (1). Poly(ε-caprolactone) (PCL) is a linear, semicrystalline, synthetic aliphatic polyester and can be biodegraded by a variety of microorganisms. PCL is one of the biomaterials used in bone repair and is regarded as a soft- and hard-tissue compatible material. This is also used in drug delivery system, resorbable suture and bone graft substitute (2). The application of PCL might be limited because of its low mechanical strength, thermal stability, gas permeability, solvent resistance, hydrophobic character, and slower resorption/degradation kinetics as compared to other polyesters. Those properties can be improved by dispersing few weight percentage of organically modified nanometer dimension clay in the matrix, by preparing nanocomposites (3–6). However, improvements in biodegradability typically come at the expense of performance and trade-offs often need to be made in achieving performance while maintaining biodegradation. Nonetheless, because of its benign degradation behavior, PCL has the potential to replace petroleum-based plastics in packaging, agricultural, and biomedical applications.

Addition of nanoparticles, such as nanoclays with ultralarge interfacial area per volume to form nanocomposites, has provided the means to improve materials performance including biodegradation. Other advantages of clay nanocomposites are their improved barrier properties while retaining the flexibility and optical clarity of the pure polymer. With a larger interfacial region along with proper organic modification, nanoclays improve the properties of the matrix polymer. The mechanical and thermal properties of PCL had been improved by blending or grafting with other thermoplastic/biodegradable polymers, such as polycarbon-

* Corresponding author. E-mail: pmaiti.mst@itbhu.ac.in.
Received for review August 28, 2009 and accepted December 7, 2009
[†] School of Materials Science and Technology, Institute of Technology, Banaras Hindu University.
[‡] Department of Zoology, Banaras Hindu University.
[§] School of Biochemical Engineering, Institute of Technology, Banaras Hindu University.
[∥] Anatomy Department, Institute of Medical Science, Banaras Hindu University.
[⊥] Indian Association for the Cultivation of Science.
DOI: 10.1021/am900584r

ate (7), polysaccharides (8), and chitosan (9). In addition, the crystal structure and structural motifs of melt crystallized PCL in the presence of nanoclay (10–12) have been reported in detail. The few weight percentage of different nanoparticles including organically modified layered silicates have improved the mechanical (12–15), thermal (11, 16–18) and gas barrier properties (19) of the matrix PCL. The thermal (16), environmental (20, 21), and enzymatic (22–27) degradation of pure PCL have also been studied during last two decades. However, the biodegradation behavior of PCL in the presence of nanoclay has not yet been studied. Moreover, the controlled biodegradation and its mechanism are the other burning issues to be resolved. The improved biodegradation of other polymer matrices (28–31) by the presence of nanoclay is reported in the literature, but the exact mechanism is yet to be revealed.

In this paper, the preparation of PCL/layered silicate nanocomposites with varying organic modifications has been reported. The improved thermal and mechanical properties along with organic-modification-dependent nanostructure of the nanocomposites have been presented. The comparative biodegradation behavior of neat PCL and nanocomposites has been examined in various media, e.g., enzyme, fungi, compost, and alkaline buffer solution, and thereby, a mechanism of biodegradation has also been revealed to establish the faster degradation rate for nanocomposites as compared to pristine polymer. Varying degradation rates in nanocomposites in the presence of two organically modified nanoclays have also been discussed. Detailed morphological studies of the biodegraded samples have been shown by using confocal, electron, and atomic force microscopy. The enhancement and/or reduction, so-called controlled biodegradation, have been explored in nanocomposites after suitably crystallizing the specimens at high temperature. All these results have been explained with the nature of interactions between the matrix polymer and organically modified nanoclay quantitatively using two different organic modifiers.

EXPERIMENTAL SECTION

Materials. Poly(ε-caprolactone) (M_w = 65 000; PDI = 1.52) from Sigma-Aldrich was used as received for this work. Two different types of organically modified nanoclays were used based on montmorillonite (Southern clay, USA, CEC 110 meq/100 g), ion-exchanged with methyl tallow bis-hydroxyethyl quaternary ammonium (30B) and dimethyl-octadecylamine (C18). The chemical structures of the organic modifiers have been shown in Scheme 1.

Nanocomposite Preparation. The organically modified nanoclay was sonicated in chloroform to achieve a good dispersion. The nanocomposites of PCL were prepared through solution route by dissolving PCL in the dispersion of nanoclay in chloroform, followed by removing the solvent at a fast rate. The solution was stirred for 30 min to ensure proper mixing. Henceforth, we will term the pure organically modified clays as 30B and C18 and their corresponding nanocomposites as PCL-30B and PCL-C18, respectively. In both the cases, 4 wt % nanoclays were used to prepare the nanocomposites.

Enzymatic Degradation. Enzymatic degradation of PCL and its nanocomposites films by Pseudomonas Lipase, type XIII, was performed at 37 °C in 50 mM potassium phosphate buffer

Scheme 1. Chemical Structures of Poly(ε-caprolactone) and Organic Modifiers Used in C18 and 30B nanoclays

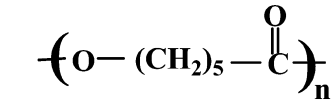

Poly(ε-caprolactone)

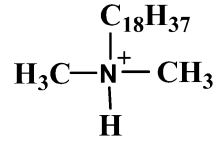

Dimethyl octadecyl ammonium salt (C18)

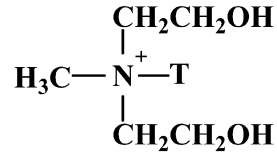

Methyl tallow bis-2-hydroxyethyl ammonium salt (30B)

(pH 7.4) containing 0.2 mg/mL Pseudomonas lipase. Initial film dimensions, 10 × 10 × 0.15 mm^3 were placed in small Viol containing 3 mL of phosphate buffer. The reaction Viol was incubated at 37 °C with constant shaking. Enzyme treatment was carried out for 6, 24, and 48 h. Samples were removed, washed with water, and dried to constant weight in vacuum before analysis.

Microorganism and Cell Culture. A fungus strain *Aspergillus fumigatus* NCIM 902 for degradation of PCL was purchased from National Chemical Laboratory, Pune. The degradation medium for fungus strain was prepared by dissolving (a) KH_2PO_4 (37.5 g), Na_2HPO_4 (69.7 g) in 1 L of water, (b) $MgSO_4 \cdot 7H_2O$ (22.5 g) in 1 L of water, (c) $CaCl_2$ (27.5 g) in 1 L of water, (d) NH_4Cl (20 g) dissolved in 1 L of water, (e) $FeSO_4 \cdot 4H_2O$ (2 g), $ZnCl_2$ (70 mg), $MnCl_2 \cdot 2H_2O$ (100 mg), H_3BO_3 (6 mg), $CoCl_2 \cdot 6H_2O$ (190 mg), $Na_2WO_4 \cdot 2H_2O$ (33 mg), $Na_2MoO_4 \cdot 2H_2O$ (36 mg), $Na_2SeO_3 \cdot 5H_2O$ (26 mg) in 10 mL of 1N HCl and added to 1 L of water, and (f) biotin (0.6 mg), vitamin B_{12} (5 mg), folic acid (2 mg), riboflavin (5 mg), and potato dextrose agar (1 mg) were dissolved in 100 mL of water. The vitamin solution was filtered and the final medium was prepared by mixing 100 mL of solution a with 1 mL of solutions b, c, e and 10 mL solution of d, and then made up to 1000 mL with deionized water to make a stock solution. Two grams of agar was added to the 100 mL of stock solution to prepare the agar gel. The polymer samples were sterilized with 5% (w/v) sodium hypochlorite solution and aseptically added to sterile agar gel. The slant of fungi was prepared by dissolving 2 g of potato dextrose agar in 50 mL of water, autoclaving for 30 min, and then allowing it to solidify for 24 h followed by the inoculation of fungi. After the growth of fungi in the slant for 4 days, it was transferred to polymer embedded agar gel.

Composting. The composted organic manure, used as inoculator, was prepared by mixing of 1:1 mixture of organic matter rich soil and cow dung. The pH of the compost was 7.0. The compost was kept wet by frequent water spraying through out the whole experiment.

Preparation of PCL Suspension. Fifty milligrams of PCL was dissolved in 15 mL of acetone at 45 °C. The PCL solution was added drop by drop in water at room temperature with vigorous stirring. Subsequently, the resulting solution was heated to remove acetone to produce PCL suspension with concentration 1.25 mg/mL. PCL suspension was used for the studies of depolymerase activity.

Assay of PCL Depolymerase Production. Potato dextrose broth 2.4 wt % in water was inoculated with *Aspergillus fumigatus* cultures grown on potato dextrose agar slant. The slant was incubated at 35 °C with constant shaking. Supernatant of experimental and control cultures were assayed for PCL depolymerase activity. PCL depolymerase activity was measured by densitometric assay using PCL suspension. The assay mixture contains 400 μL of PCL suspension (1.25 mg/mL), 50 mM potassium phosphate buffer (1.3 mL), and culture supernatant (300 μL). PCL depolymerase activity and biodegradation were measured from optical density data as a function of time. The supernatant from those cultures were analyzed for depolymerase activity at different pH values. Potassium phosphate buffers (50 mM) at pH 5.5, 6.6, 8.2, 9, and 10 were used in the depolymerase assay.

Biodegradation Studies. Biodegradation of PCL and its nanocomposites was studied with the samples crystallized at different temperatures (room temperature quenched, 45° and 52 °C) in a sealed chamber at constant humidity of ~85% at 35 °C. Enzyme, pure microorganisms (fungi), composted manure, distilled water, and alkaline buffer were used as the biodegradation media. Test specimens ($10 \times 10 \times 1$ mm^3) were prepared from compression-molded samples after quenching to room temperature, to maximize the amorphous content. The effect of crystallinity on biodegradation was also studied with samples crystallized at different temperatures. The sheets of specimens were crystallized at 45 and 52 °C for 24 and 48 h, respectively, in hot stage, ensuring complete crystallization from impinging of spherulites to make different crystallinity content and spherulite size. The percentage weight loss after compost burial/other media was considered as the measure of biodegradation.

X-ray Diffraction (XRD). X-ray diffraction experiments were performed using a Bruker AXS D8 Advance wide-angle X-ray diffractometer with Cu Kα radiation and a graphite monochromator (wavelength, $\lambda = 0.154$ nm). The generator was operated at 40 kV and 20 mA. The thin sheet of the samples was placed on a glass sample holder at room temperature and scanned at diffraction angle 2θ from 1 to 40° at a scanning rate of 1°/ min.

Thermal Characterization. The melting, crystallization temperatures and heats of fusion of freshly prepared nanocomposites and pure PCL films have been measured in a Mettler 832 DSC instrument. The samples were heated at the scan rate of 10 °C/min. The peak temperature and enthalpy of fusion were calculated from the endotherms using a computer attached with the instrument. After the first melting, the samples were cooled down at a constant rate of 10 °C /min to find the crystallization temperature and heat of crystallization in a similar fashion. The melting temperature and the heat of fusion of the biodegraded samples have been measured in the same way. Isothermal crystallizations have been carried out inside DSC for the measurement of the equilibrium melting temperatures. The samples were initially melted at 90 °C for 5 min and then quenched at the rate of 100 °C/min to the predetermined isothermal temperature. Crystallizations have been performed for different times at different temperatures. The samples were melted at the heating rate of 10 °C/min from the isothermal crystallization temperature to 90 °C without cooling. The DSC was calibrated with indium and zinc before use.

Mechanical Properties. ***Dynamic Mechanical Characterization.*** Frequency dependence of oscillatory shear moduli in the liquid state was measured, using dynamic frequency sweep tests, on Rheologica (model: Nova) using parallel plate geometry (25 mm) at various temperatures between 70 and 190 °C, keeping the strain amplitude of 0.05 to maintain the linear response of the sample. The measured angular frequency ω for oscillatory shear experiment was kept in the range of 0.5 to 100 rad/s. The time−temperature superposition principle was applied to frequency-dependence moduli at different temperatures in an attempt to determine the linear viscoelastic properties over a wide range of time scale. The storage moduli and complex viscosities were measured as a function of reduced angular frequency for pure PCL and its nanocomposites. Steady shear viscosity was measured in the liquid state using cone−plate geometry at 90 °C with the shear rate of 0.01 s^{-1}.

Tensile Modulus. Tensile tests were performed with the injection-molded samples using an Instron 3369 tensile tester at a strain rate of 5 mm min^{-1} at room temperature. Several samples were tested to obtain good error estimates.

Morphological Investigation. The nanoclay dispersion in the matrix was checked by using TEM (Technai G^2) operated at an accelerating voltage of 100 kV. A thin layer, around 70 nm thick, from the nanocomposite sample was sectioned at −80.0 °C using a Leica ultramicrotome equipped with a sharp glass knife. The surface morphology of pure PCL and its nanocomposites was investigated by using both scanning electron microscope (SEM) and atomic force microscope (AFM). The surface morphology of the samples was examined with a LEO 435 VP instrument operated at 15 kV. All the samples were gold-coated by means of a sputtering apparatus before observation. Atomic force microscope was performed using a NT-MDT multimode AFM, Russia, controlled by Solver scanning probe microscope. Semicontact mode was used with the tip mounted on 100 μm long, single-beam cantilever with resonance frequency in the rage of 240−255 kHz, and the corresponding spring constant of 11.5 N/m. The roughness of the surfaces caused by biodegradation was also examined by using SEM and AFM. The spherulitic morphology was examined using a polarizing optical microscope (POM) (Leitz) after crystallizing the samples at 52 °C for 48 h on a Mettler hot stage. To check the shape and size of the samples before and after biodegradation, we took the photographs of the samples using a digital camera. To observe the morphology of the PCL sheet and its nanocomposites in Z-section before and after biodegradation, we stained the samples with Rhodamine B and scanned them under Zeiss LSM 510 Meta laser scanning confocal microscope.

RESULTS AND DISCUSSION

Nanostructure. Figure 1 compares the *X*-ray diffraction patterns of pure organoclays (30B and C18) and their respective nanocomposites. A shift in the diffraction peak has been observed toward lower angle for PCL-C18 nanocomposite as compared to pure C18, suggesting the pattern of an intercalated nanostructure due to the insertion of polymer chains inside the clay gallery. The d_{001}-spacings for pure C18 and PCL-C18 have been calculated to be 2.45 and 3.3 nm, respectively. On the other hand, the strong (001) peak of pristine 30B clay at ~4.8° 2θ has disappeared in the nanocomposite, indicating an exfoliated/disordered nanostructure for PCL-30B nanocomposite. The nanostructure is very different depending on the organic modifier used in organoclay. The exfoliated or highly disordered nanostructure of PCL-30B is presumably due to the greater interactions

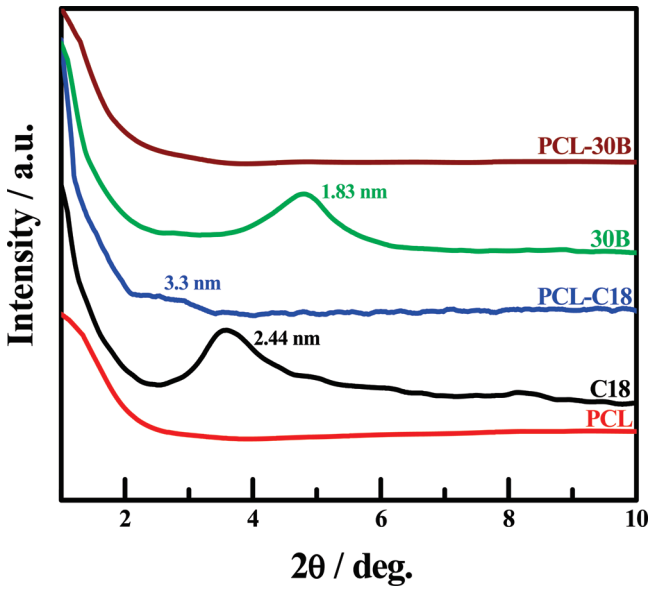

FIGURE 1. Wide-angle X-ray diffraction patterns of indicated organically modified nanoclays and PCL nanocomposites. The numbers in nanometers represent the gallery spacing calculated from Bragg's equation.

Table 1. Characteristics of Pure PCL, Nanoclays, And Their Nanocomposites

sample	M_W	d_{001} (nm)	D_{hkl} (nm)	T_m (°C)	ΔH_m (J g^{-1})	T_c (°C)	ΔH_c (J g^{-1})
PCL	65 000			55.7	69.0	26.4	63.0
C18		2.44	17.4				
PCL-C18	65 000	3.3	22.9	56.4	64.0	30.9	56.0
30B		1.83	18.56				
PCL-30B	65 000			56.2	60.0	30.2	53.5

between the matrix PCL and 30B organoclay as compared to PCL and C18. Pure PCL has no peak within the 2θ range of 1−10°, as it does not have any nanostructure. PCL-C18 nanocomposite exhibits higher order of the silicate layers (22.9 nm) against pure organoclay (17.4 nm), as calculated from the Scherrer equation, $D_{hkl} = (k\lambda)/(\beta\cos\theta)$, where k = constant, λ = wavelength of X-ray used, β = full width at half maxima, and θ = peak angle of (001) reflection (Table 1) (32, 33).

The nature of dispersion of the nanoclay in PCL-C18 and PCL-30B nanocomposites has been shown in Figure 2. The TEM images (low-magnification) confirm the presence of intercalated hybrids for both the nanocomposites. Highly disordered structure of PCL-30B has also been confirmed from the absence of any intercalated peak in XRD pattern. On the other hand, the C18 nanoclay forms a network structure in PCL-C18 nanocomposite through the linkages of hydroxyl groups present in the edges, so-called flocculation, whereas its intercalated pattern has been confirmed from the high-magnification image (Figure 2c). Further high-magnification TEM image shows the intercalation of polymer inside the silicate galleries (Figure 2d). The correlation lengths of the nanoclay are found to be 40 nm and 1.3 μm for PCL-30B and PCL-C18 nanocomposites, respectively, demonstrating the very different distribution of nanoclay in the matrix.

Figure 3 shows the XRD patterns (crystalline structure) of pristine PCL and its nanocomposites of matching film thickness. The orthorhombic crystalline structure of PCL (11) is retained in nanocomposites in presence of nanoclays while the peak intensities have been reduced in nanocomposites as compared to pristine PCL, exhibiting less crystallinity because some sort of interactions develop in nanocomposites. The peak intensity of PCL-30B has been lowered compared to PCL-C18, suggesting stronger interaction between PCL and 30B than that of the PCL-C18 nanocomposite. However, PCL nanocomposites are intercalated and the crystalline structure remains intact in presence of disklike nanoclays.

Thermal Behavior. The representative DSC traces of the solution cast samples of neat PCL and its nanocomposites have been shown in Figure 4a. Both pristine PCL and nanocomposites exhibit distinct endothermic melting peaks (T_m) at 55.7, 56.3, and 56.4 °C for PCL, PCL-C18, and PCL-30B, respectively. The heat of fusion (ΔH) decreases in nanocomposites in the presence of nanoclays (69, 64, and 60 J/g for pristine PCL, PCL-C18, and PCL-30B, respectively) because of interaction between polymer and nanoclays. The extent of interaction is more in case of PCL-30B nanocomposite as revealed from the lowest heat of fusion and lowering of melting temperature. The cooling curves exhibit an increase in crystallization temperature (T_c) for nanocomposites as compared to pristine PCL. The crystallization peak is slightly broad for pristine PCL against a rather sharp peak for nanocomposites (Figure 4b). The shifting of T_c to 31 °C for nanocomposites against 26 °C broader peak for pure *PCL* suggests that the clay particles act as nucleating agent (32). The nanocomposites also appear to be less crystalline during cooling as compared to neat polymer (ΔH_c = 63, 56, and 54 J/g for PCL, PCL-C18, and PCL-30B, respectively). The nucleating phenomena have also been observed in polarizing optical micrographs. The average spherulitic diameters were 120, 70, and 80 μm for pure PCL, PCL-C18, and PCL-30B, respectively (Figure 5).Both the organoclays act as nucleating agents, whereas the enhanced interaction in PCL-30B restricts the crystal growth rate of the matrix, providing a bit larger spherulites as compared to PCL-C18 nanocomposite after full solidification.

Mechanical Properties. The comparison of storage modulus $G'(\omega)$ against reduced angular frequency $a_T\omega$ for pure PCL and its nanocomposites with the reference temperature T_{ref} (= 110 °C) has been shown in Figure 6a, where, a_T is the WLF-type shift factor determined from dynamic moduli (34). The values of $G'(\omega)$ have increased for nanocomposites with respect to pure PCL indicating greater chain stiffness of the matrix PCL in presence of layered silicate. In the lower ω region, the curves can be expressed by a power-law of $G'(\omega) \propto \omega^{1.3}$ for PCL, instead of typical $G'(\omega) \propto \omega^2$ for narrow molecular weight distribution of homopolymer melt, while both the nanocomposites exhibit further

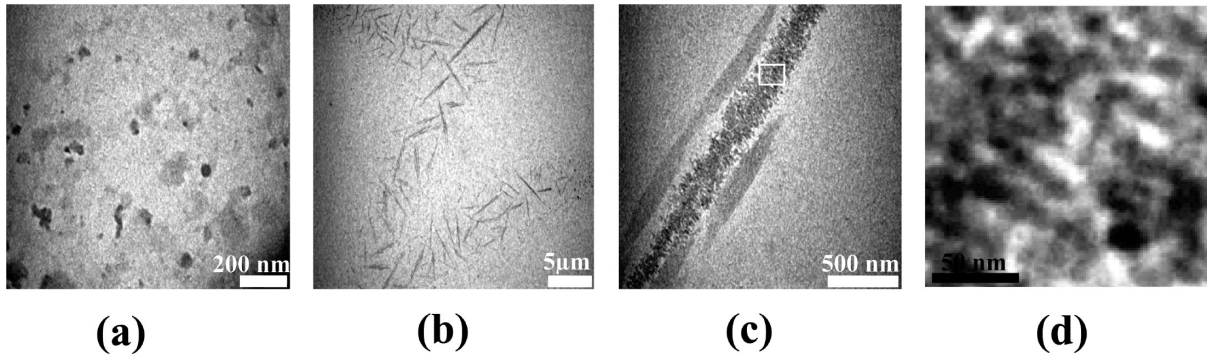

FIGURE 2. Bright-field transmission electron micrographs of nanocomposites (4 wt % clay) (a) PCL-30B, (b) PCL-C18 (low-magnification), (c) PCL-C18 (high-magnification), and (d) high-magnification image of the indicated region in c.

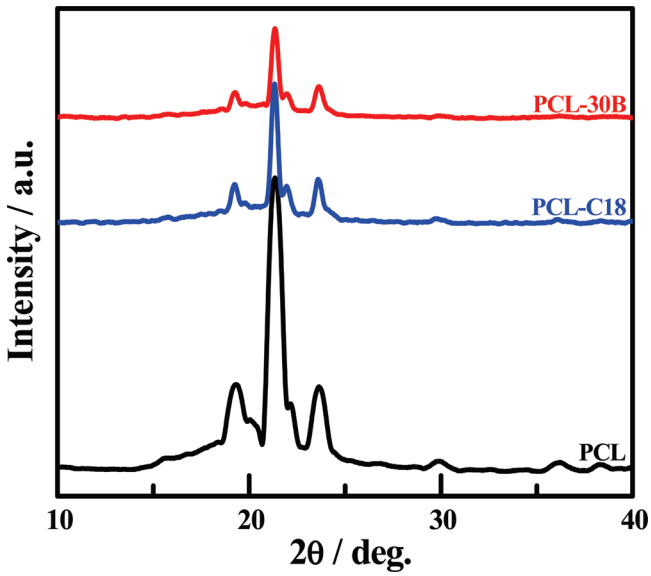

FIGURE 3. XRD patterns of pure PCL and its indicated nanocomposites. The *Y*-axis has been shifted for the clarity of presentation.

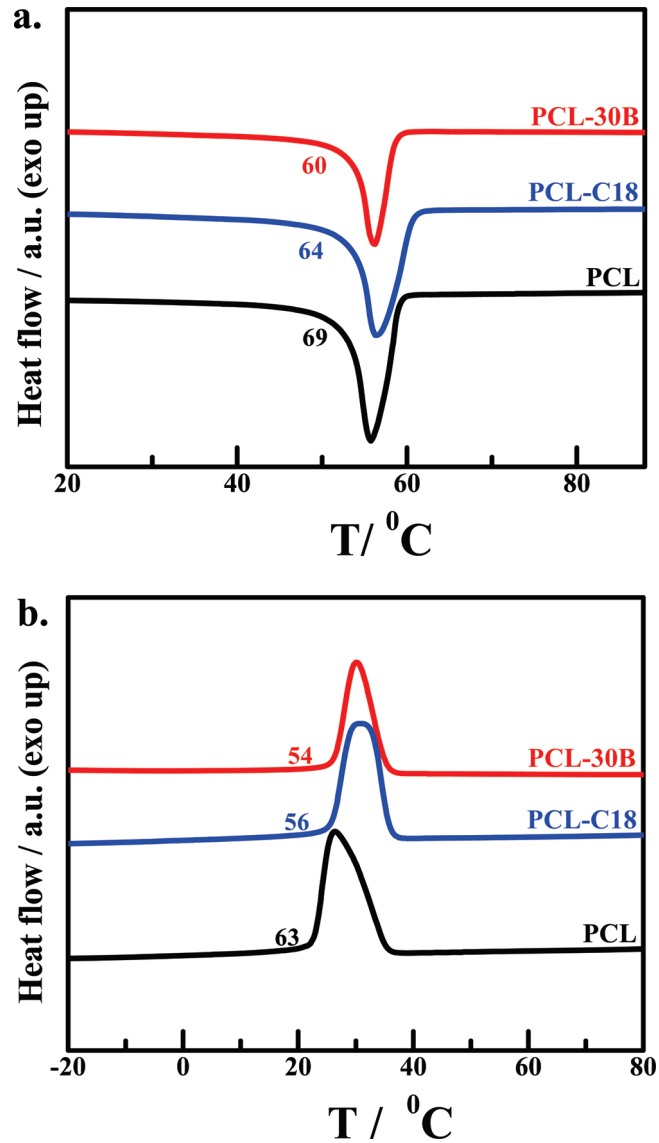

FIGURE 4. DSC thermograms of PCL and its indicated nanocomposites: (a) heating curves, (b) cooling curves. The numbers represent the heat of fusion in a, and heat of crystallization in b in J/g units.

lower ω dependence (1.2 for PCL-C18 and PCL-30B) showing more pseudosolid like behavior in nanocomposites. The inset in the panel represents the plot of log a_T versus T. Almost similar values of shift factor on clay loading suggest that the temperature dependent relaxation process observed are basically unaffected by the presence of nanoclay (35). The complex viscosities of the nanocomposites, $|\eta^*|$, are also higher than that of pure PCL, because of the greater stiffness of PCL chains in the presence of layered silicates (Figure 6b). The higher reinforcement in PCL-C18 as compared to PCL-30B might be due to the network structure present in the PCL-C18 system as evident from the TEM image (Figure 2b). The melt viscosities in the steady shear experiment also exhibit the similar trend (Figure 6c). Hence, the mechanical properties of the nanocomposites in melt phase have improved with respect to pure PCL.

The stress–strain curves of pure PCL and its nanocomposites in solid state have been shown in Figure 7. The tensile moduli, calculated from the initial linear slopes, have increased significantly for nanocomposites as compared to pure *PCL*. The tensile moduli are 382, 563, and 485 MPa for pure PCL, PCL-C18 and PCL-30B, respectively. In addition, the toughness (area under the stress–strain curve) of PCL-C18 is higher than that of pure PCL-30B nanocomposites (36). The superior mechanical properties of PCL-C18 are significantly higher as compared to those in the PCL-30B

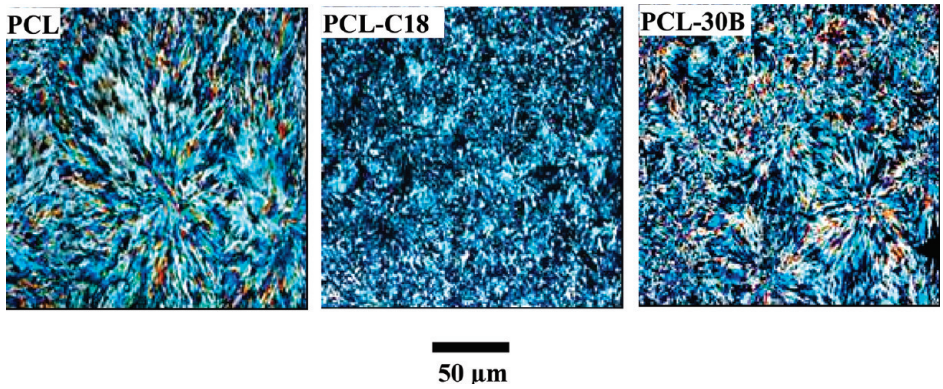

FIGURE 5. Polarizing optical images of PCL and its indicated nanocomposites. The samples were crystallized at 52 °C up to full solidification.

system for the same reason as discussed above for the liquid state. Contrary to the conventional notion, highly intercalated nanocomposite exhibits better mechanical properties than that of partially exfoliated/disordered system, which can be explained from the sandwiched effect of polymer chains inside the silicate galleries.

Biodegradation. Biodegradation tests have been carried out at 30 °C with the samples quenched to room temperature in enzyme media (lipase type XIII from Pseudomonas sp. in buffer solution). The enzymatic degradation rates of nanocomposites are much faster than that of pure PCL (Figure 8a) and among the nanocomposites, PCL-30B exhibits higher degradation rate than that of PCL-C18. The matrix PCL degrades at a regulated higher rate in the presence of organically modified nanoclay, raising a clay dependency phenomenon. The morphology as observed in scanning confocal images (Figure 8b) also exhibits the highest enzymatic degradation in PCL-30B and the lowest in pure PCL. The morphology at various Z-sections of the specimen also supports the similar nature of degradation as seen in confocal images. Though perforated images are evident from PCL-30B, small holes are observed in pure PCL after biodegradation. The phase contrast images of pristine PCL and its nanocomposites (before and after enzymatic degradation) also support the relative degradation rate (Figure 8c) of pure polymer and different nanocomposites. Studies have been carried out to observe the effect of nanoclay on biodegradation rate of PCL in a microorganism (fungi: *Aspergillus fumigatus-NCIM 902*) medium. A marked increase in biodegradation rate has been observed for PCL-30B nanocomposite (more than 90% weight loss) in pure fungi medium as compared to pristine PCL (~40 wt %) (Figure 9a). Moreover, the rate of biodegradation of PCL-30B is higher as compared to PCL-C18, the same trend we observed in the case of enzymatic degradation. Biodegradation of up to 95% weight loss has been achieved, as the sample recovery was relatively easier in pure fungi medium and the integrity of the sample was quite fair as compared to compost degraded specimens discussed below. The optical images of the specimens before and after biodegradation in fungi medium have been presented in Figure 9b, showing much less damage/loss of samples for pure PCL, whereas severe weight loss has occurred in nanocomposites, as expected from the kinetics of the biodegradation experiment (Figure 8a). The thickness of the pure PCL film decreases, causing a 40% weight loss in 75 days even though the dimension remains almost same after biodegradation.

The changes in weight loss due to biodegradation in compost manure have been shown in Figure 10a. The rate of biodegradation is quite slow for pristine PCL, ca. ~50 wt % degradation in 60 days. On the other hand, the biodegradation rate has enhanced significantly in nanocomposites in presence of nanoclays with 63 and 83 wt % loss observed in the same time for PCL-C18 and PCL-30B, respectively. The biodegradation studies had been stopped after 60 days as the nanocomposites samples become brittle and difficult to recover from the compost. Nonetheless, the biodegradation rate of matrix polymer can be tuned by dispersing suitable nanoclays into it. The higher degradation rate in presence of nanoclay is attributed to the presence of hydroxyl groups on the edges of montmorillonite, which can catalyze faster hydrolytic degradation of the matrix polymer (37). Comparatively higher biodegradation rate of PCL-30B nanocomposite is presumably due to the greater interaction between PCL and 30B nanoclay, as evident from the lowest heat of fusion/crystallinity (Figures 3 and 4) against PCL-C18 nanocomposite. In addition, the presence of excess hydroxyl ions present in the organic modifier of 30B nanoclay may accelerate the hydrolytic decomposition vis-à-vis C18 nanoclay, where methyl and octadecyl groups are at hand in the organic modifier.

The biodegradation rate has significantly been suppressed in bioreactive Ganges water at room temperature (see the Supporting Information, Figure S1) with the same dimension of samples ~($1 \times 1 \times 0.1$ cm^3) used in compost or other media. Only 20% weight loss has been observed after 200 days of exposure. Here again, the biodegradation rates of the nanocomposites have increased slightly with respect to pure PCL. In contrast, the overall biodegradation for all the samples were low as compared to the degradation rate in other media, primarily because of the lower abundance of specific microorganism necessary to hydrolyze PCL present in the Ganges water. It is worth mentioning here that the biodegradation experiment has also been carried out in distilled water both for pure PCL and its nanocomposites. Surprisingly, weight loss has not occurred for pure PCL and

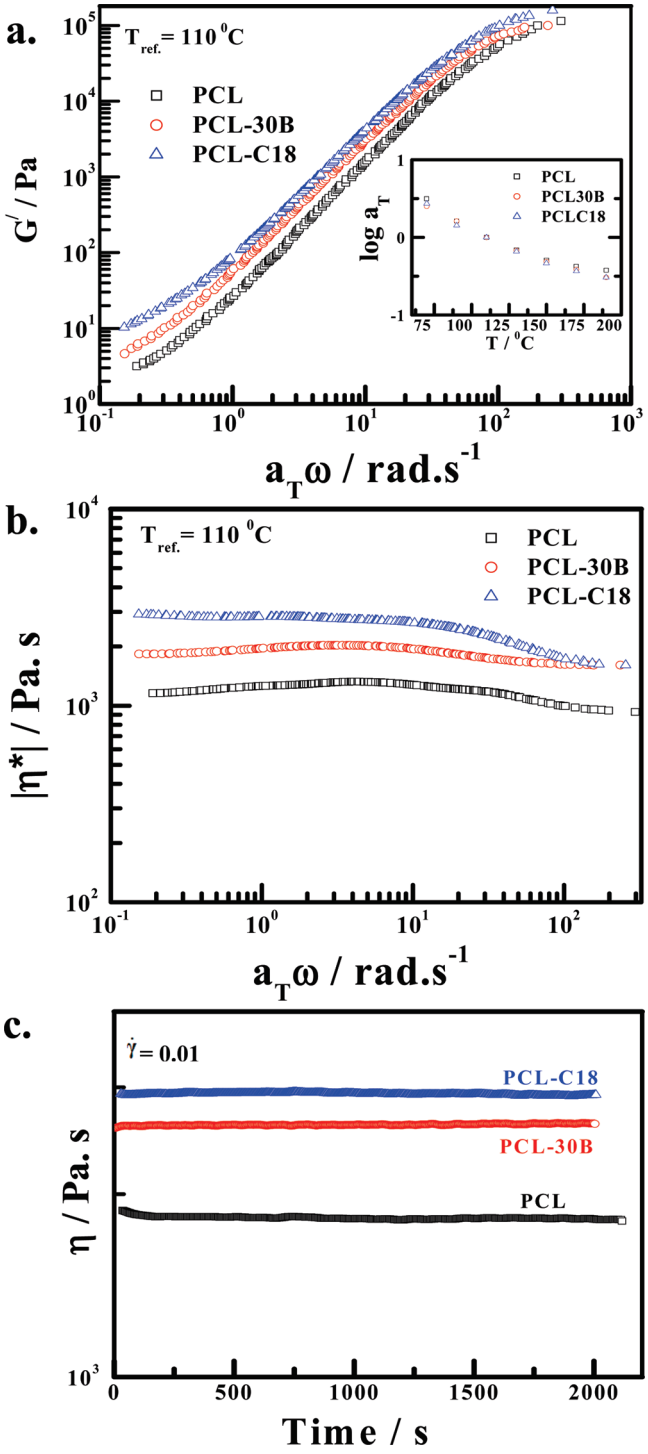

FIGURE 6. Reduced frequency dependency of (a) storage modulus and (b) complex viscosity of pure PCL and its indicated nanocomposites at T_{ref} = 110 °C. The inset panel shows the shift factor, a_T against temperature plot and (c) steady shear viscosity at constant shear rate as mentioned.

its nanocomposites up to 200 days of exposure at 30 °C. So, the presence of microorganism is a precondition for starting the hydrolysis and subsequent biodegradation. The PCLs have been shown to be degraded by enzymes secreted by a number of bacterias, yeasts and fungis (38–40). The surface roughening due to biodegradation has been shown using SEM micrographs of pure PCL and its nanocomposites in compost manure (Figure 10b) showing greater loss of

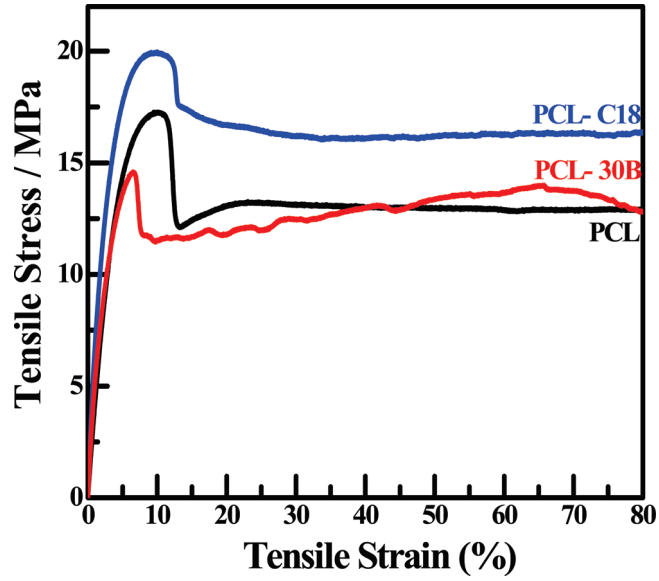

FIGURE 7. Stress–strain curves for pure PCL and its nanocomposites with the elongation rate as 5 mm/min.

samples from the surfaces as bigger pits are observed in nanocomposites as compared to pristine PCL. Furthermore, the pittings appeared in excess in PCL-30B than that of PCL-C18 nanocomposite for the same time of exposure (60 days). Both PCL and its nanocomposites do not exhibit any pitting before biodegradation. So, surface roughening occurred in greater extent in nanocomposites due to enhanced biodegradation with respect to pristine PCL. The globular pattern was observed for pure PCL, whereas striations were seen in case of PCL-30B and PCL-C18 nanocomposites as revealed through AFM tapping mode micrographs (Figure 10c). The striation pattern in the matrix has been generated by the disklike layered silicate with aspect ratio ~250. The surface morphology has changed significantly just after 20 days of biodegradation, exhibiting hillocks of globules in pure PCL as some parts of polymer surfaces have been eaten up by the microorganism. In contrast, the surface morphology becomes patchier in nanocomposite in presence of layered silicates as evident from the vertical scale (height profile) of ~2 μm against the value of ~1 μm in pure PCL. On the other hand, the surface roughness was around 500 nm both for pure PCL and nanocomposites before degradation. The greater irregularities of the surfaces of the nanocomposite as compared to pure PCL after biodegradation arise from the greater extent of biodegradation in nanocomposites, which we observed quantitatively in Figure 10a. The unevenness of the samples after biodegradation restricts AFM measurement, thereby, exhibiting blank portion in the micrographs. This is the reason why we could not observe any AFM micrographs for highly biodegraded samples. However, significant loss of materials from its surfaces as evident from the pittings have clearly been shown in optical images, SEM and AFM, and scanning confocal micrographs because of biodegradation, and the greater losses occurred for nanocomposites vis-à-vis pure PCL.

Controlled Biodegradation. The biodegradation rates of PCL have been presented with and without the

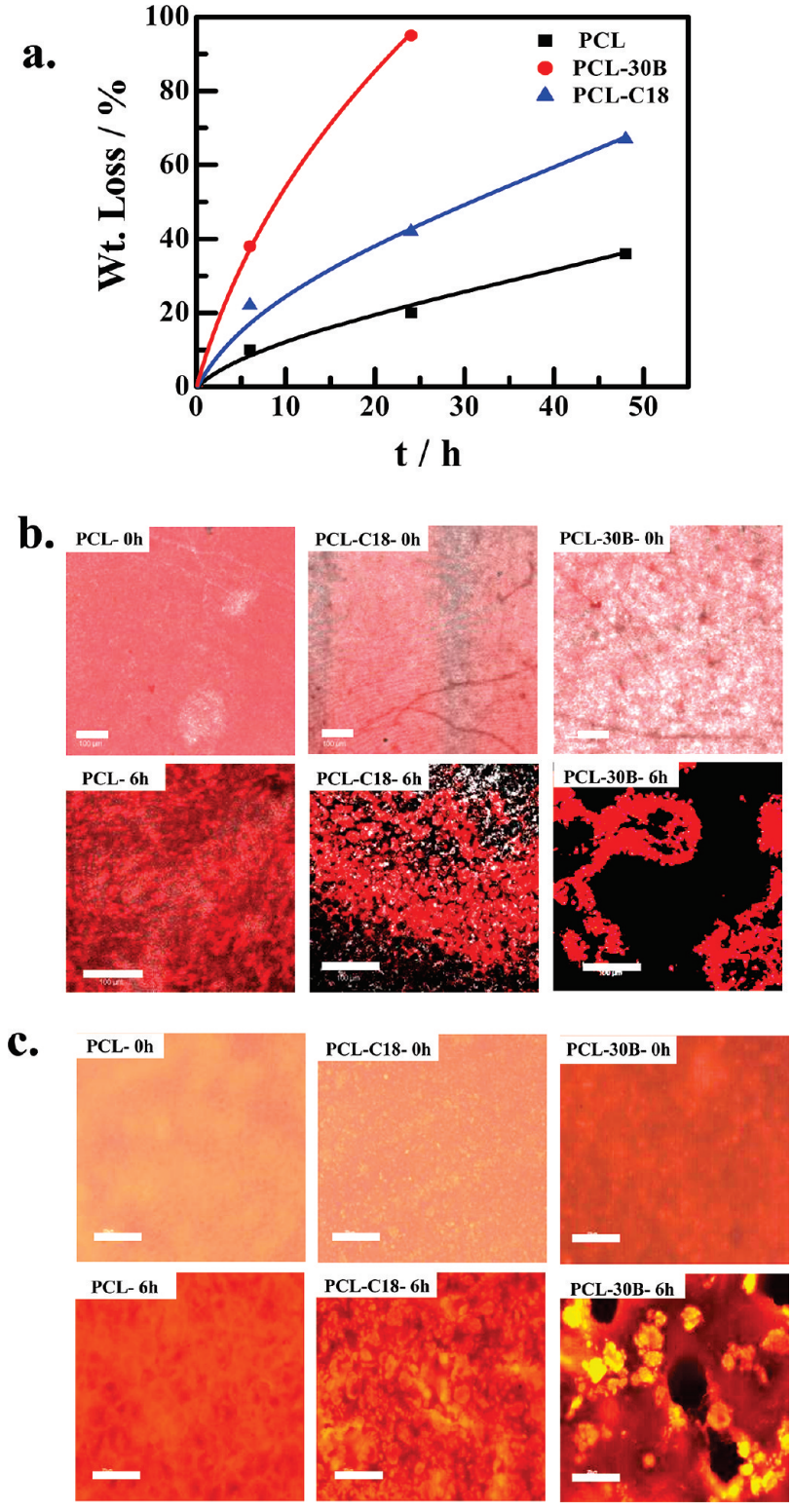

FIGURE 8. (a) Percentage weight loss of PCL and its indicated nanocomposites during enzymatic (lipase from Pseudomonas sp., Type XIII) degradation at 37 °C. (b) LCM images of PCL and its indicated nanocomposites (scale bar = 100 μm). (c) Phase contrast images of PCL and its indicated nanocomposites (scale bar = 50 μm). The numbers after the specimen name represent the biodegradation time in hours. The number "0" indicates the sample before starting enzymatic degradation.

presence of nanoclays. The regulated biodegradation is another tropical interest. In other words, it is necessary to decrease or increase the rate of biodegradation of polymer apart from its natural degradation. The biodegradation rates of PCL and representative PCL-C18 nanocomposite samples quenched to room temperature and crystallized at 52 °C up to full solidification (48 h crystallization) have been shown in Figure 11. The biodegradation rate has significantly been reduced for the samples crystallized at 52 °C as compared to room temperature quenched samples both for pure PCL

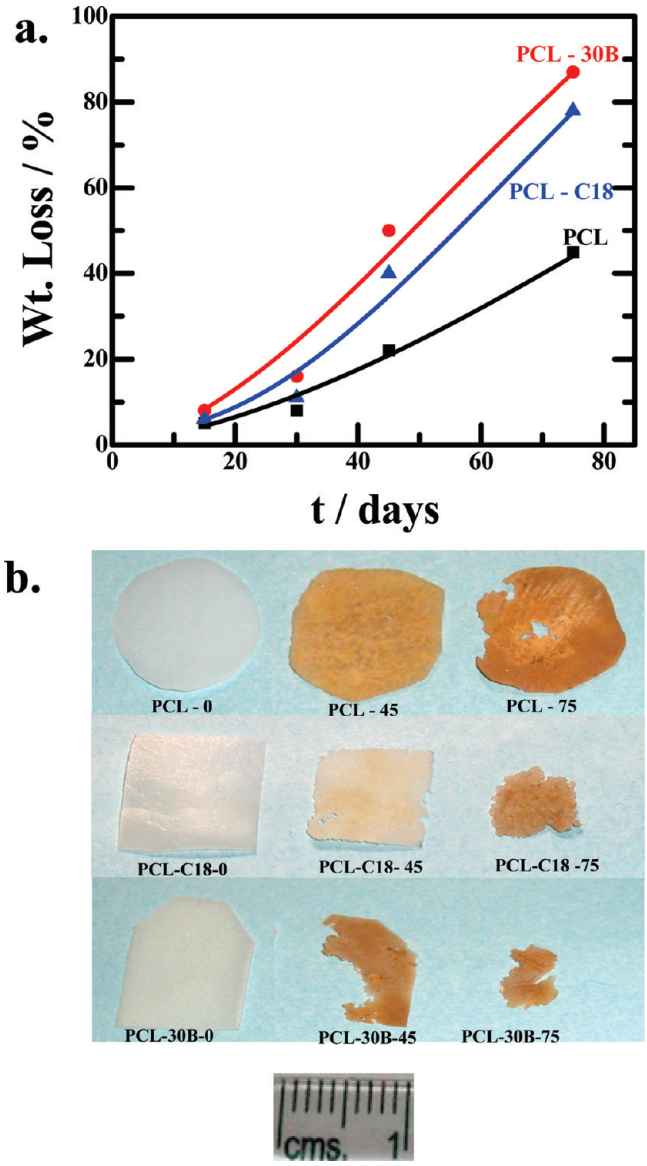

FIGURE 9. (a) Percentage weight loss of PCL and its indicated nanocomposites during biodegradation at room temperature in pure fungi medium. (b) Optical micrographs of PCL and its indicated nanocomposites before and after biodegradation in fungi medium. The last numbers (0, 45, and 75) represent the days of exposure in biodegradation (fungi) medium. The number "0" indicates the sample before starting biodegradation. The shapes of the samples were so chosen that after exposure we could locate the individual samples as they were put together in single media in order to keep the environment the same. The scale has been given to show the dimensions of the film used for biodegradation and their shapes after biodegradation for various times.

and its nanocomposite. Nevertheless, the rate of biodegradation has always improved for nanocomposite as compared to neat PCL for a particular thermal history. The samples crystallized at 45 °C exhibit higher degradation rate than that of samples crystallized at 52 °C, but it exhibit lower rate than room temperature quenched samples both for pristine PCL and its nanocomposite (see the Supporting Information, Figure S2). Other nanocomposite, namely PCL-30B, also exhibits similar biodegradation behavior depending on thermal treatment. The sluggish biodegradation rate of the samples crystallized at higher temperature might be due to the higher amount of crystallinity as evident from the higher heats of fusion and bigger size of spherulites (36). The biodegradation rate has decreased by ~25−35% with increasing crystallization temperature from 30 to 52 °C. Usually, the biodegradation starts in the amorphous region (41), and it is reasonable to expect the rate of biodegradation to be more sluggish for samples with a greater amount of crystallinity and bigger spherulite dimension (42–44). The measurement of molecular weight by using GPC shows that the molecular weight is almost the same (see the Supporting Information, Figure S3) before and after biodegradation both for pure PCL and its nanocomposites, indicating that the biodegradation phenomena occurred initially in the amorphous region (45, 46). In principle, the reduction of biodegradation rate of PCL as compared to its natural degradation rate was made possible by suitably crystallizing the pure polymer and its nanocomposites. Thereby, one can fine-tune the rate of biodegradation to either increase or decrease with respect to natural degradation rate.

Biodegradation Mechanism. To explore the mechanism of biodegradation, heats of fusion of samples have been measured at various stages of biodegradation. Figure 12 shows the heat of fusion (ΔH) for pristine PCL and its nanocomposites with biodegradation time, measured for room temperature quenched samples. The ΔH is lower for the nanocomposites as compared to neat PCL before starting biodegradation as a result of enhanced interaction between PCL and nanoclay. High amorphous content along with the catalytic effect of clay, as mentioned earlier, may enhance the biodegradation rate of nanocomposites as compared to pristine PCL. Figure 12 also shows that the heat of fusion increases sharply with biodegradation time for the nanocomposites, whereas there is only a slight increase for neat PCL after 6 weeks of biodegradation. The rapid increase in ΔH indicates that the amorphous part is first attacked/eaten up by the enzyme/microorganisms causing more crystalline materials remain in the samples. As the biodegradation starts in the amorphous region, it is rational to expect the rate of biodegradation to be more sluggish for samples with a high amount of crystallinity. Further, it is well-known that the activity of enzymes (mostly depolymerase), secreted by microorganism, plays an active role to degrade the polymer. Murphy et al. showed that the depolymerase activity of the enzyme (PCL-depolymerase extracted from *Fusarium solani*) is enhanced in slightly basic medium (pH ~8.0) (24). The measurement of pH of clay solutions (4 wt %) in water has shown 7.5 and 8.4 for C18 and 30B nanoclay, respectively. The depolymerase activity, calculated from optical density measurement of *PCL* colloidal solution using enzyme extracted from fungi (*Aspergillus fumigatus*), has been presented in Figure 13 as a function of pH. Depolymerase activity increases with increasing pH of the solution, indicating higher activity of the enzyme in alkaline media. Therefore, the greater enzyme (PCL-depolymerase) activity in slight alkaline nanocomposite caused higher biodegradation in presence of nanoparticles. It is worth mentioning here that pH of PCL solution was 7.0. Higher pH (8.4) in PCL-30B

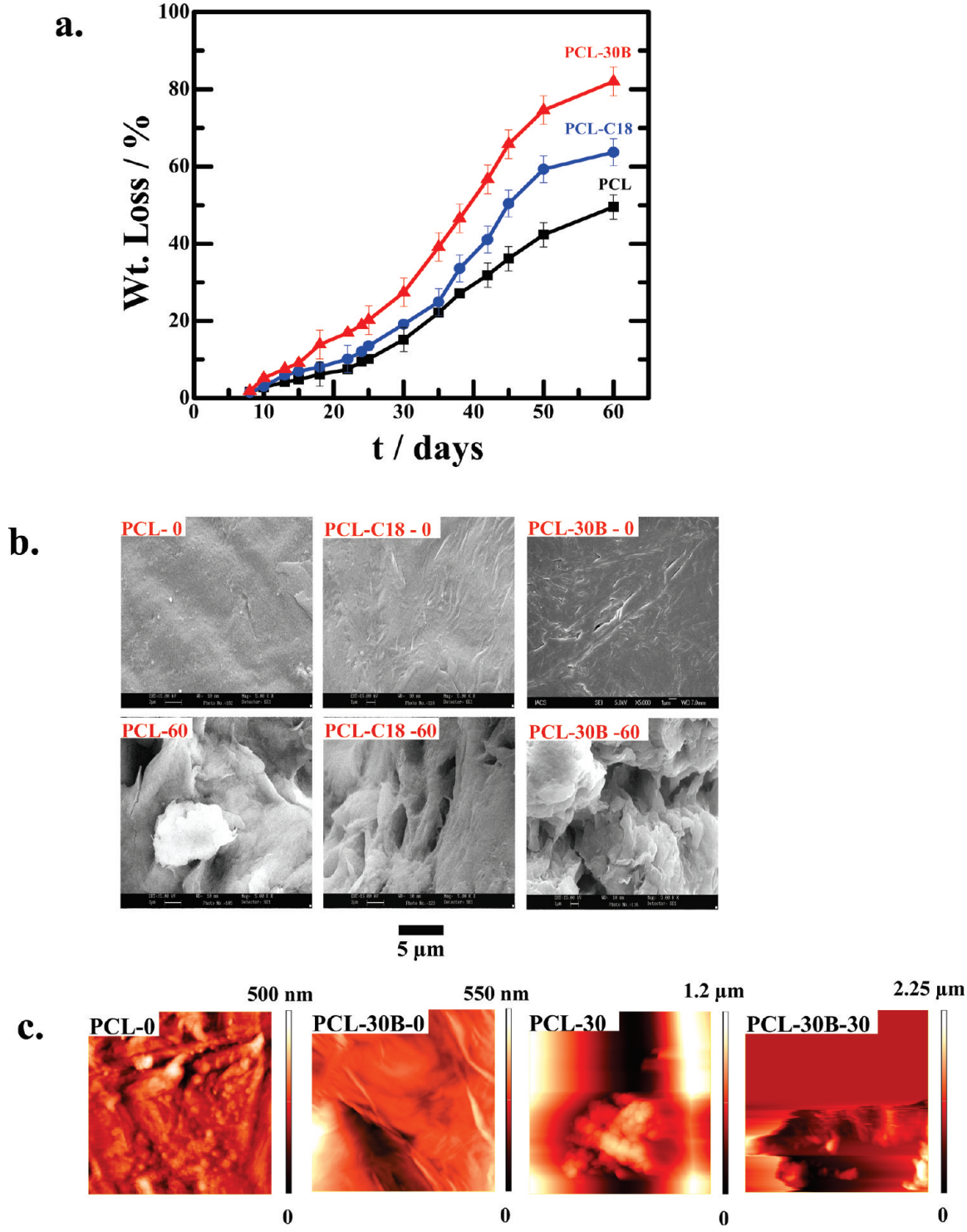

FIGURE 10. (a) Percentage weight loss of PCL and its indicated nanocomposites during biodegradation at room temperature in compost medium. (b) FE-SEM images of PCL and its indicated nanocomposites. (c) AFM images of PCL and its indicated nanocomposites thin film (12 μm $\times$ 12 μm) before and after biodegradation obtained in tapping mode. Height profile is given after each image. The numbers after the specimens name represent the biodegradation time in days. The number "0" indicates the sample before starting biodegradation or pristine samples.

nanocomposite explains the higher biodegradation rate as compared to PCL-C18 nanocomposite (pH ~7.5). Therefore, the enhanced enzymatic activity in nanocomposites, due to alkaline pH together with higher amorphous content, increased the rate of biodegradation relative to that of pure PCL and the relative higher rate in PCL-30B nanocomposite is well-explained on the basis of higher alkalinity and lower crystallinity as compared to the PCL-C18 nanocomposite. To show the effect of alkalinity on biodegradation, we have measured the rates in alkaline buffer (pH ~9) solution (in the absence of any microorganism). The biodegradation was restricted up to ~2 wt % only even after 100 days of exposure both for pristine PCL and its nanocomposites. So, the presence of microorganism is necessary for initiating the biodegradation and the activity of enzyme gets enhanced

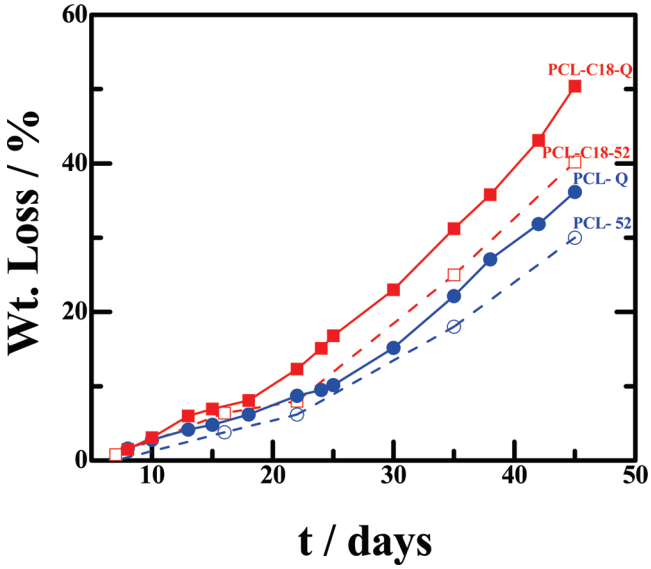

FIGURE 11. Percentage weight loss of PCL and its indicated nanocomposites during biodegradation at room temperature in the compost media. "Q" represents the samples quenched to RT and "52" represents the samples crystallized at 52 °C.

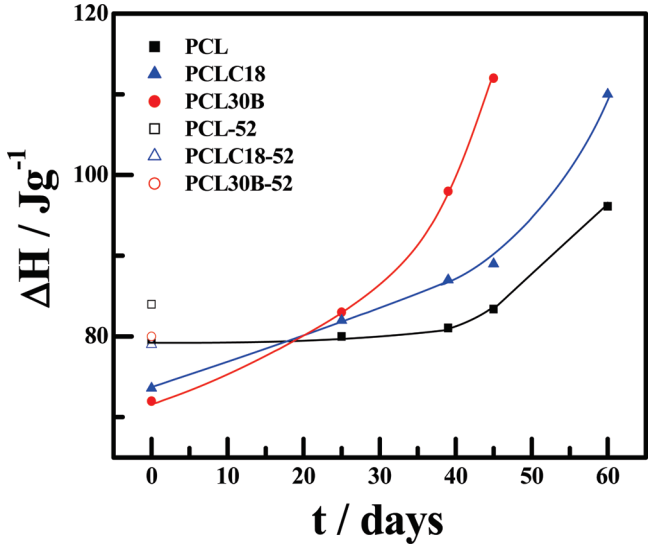

FIGURE 12. Heats of fusion as a function of biodegradation time for pure PCL and its indicated nanocomposites. The solid lines are guide to the eye. The solid symbols are for room temperature quenched samples and open symbols are for the samples crystallized at 52 °C for 48 h (before starting biodegradation).

in alkaline condition causing higher biodegradation rate in nanocomposites as compared to pure PCL.

Interactions in Nanocomposites. We have witnessed the improvement in properties including biodegradation of the nanocomposites. Moreover, the enhancement in case of PCL-30B is higher than that of PCL-C18 especially for biodegradation. This difference might be due to the varying extent of interaction between matrix PCL and 30B/C18 organoclays. To quantify the interactions between polymer and nanoclays, we have taken into account the interaction parameter (χ), by using the depression of melting point of PCL in presence of nanoclay, following the equation of Nishi and Wang (47)

$$\frac{1}{T_{NC}^{o}} - \frac{1}{T_{PCL}^{o}} = -\frac{RV_{PCL}}{\Delta H_u V_{clay}}\phi_{clay}^{2}\chi \qquad (1)$$

where, T_{NC}^{o} and T_{PCL}^{o} are the equilibrium melting points of the nanocomposite and that of the pure PCL, respectively. V_{PCL} and V_{clay} are the molar volumes of the repeating unit of PCL and the molar volume organoclay, respectively, ϕ_{clay} is the volume fraction of clay, and ΔH_u is the enthalpy of fusion per mole of repeating unit of PCL. The extrapolation technique of $T_m - T_c$ plot to the $T_m = T_c$ line (Hoffman–Weeks plot) (48) has been used to measure the equilibrium melting point. Figure 14a shows the representative plot of melting point against heat of fusion of pure PCL crystallized at different temperatures mentioned for various time. The melting point increases with increasing crystallization temperature (T_c) and this phenomena is followed for the nanocomposites as well. The $T_m - T_c$ plot has been shown in Figure 14b, where the melting points of the nanocomposites are slightly lower than that of pure PCL for any particular T_c. The equilibrium melting points, T_m^o of pure PCL and its nanocomposites have been evaluated after extrapolation to $T_m = T_c$ line and the values are 72, 68, and 64 °C for neat PCL, PCL-C18, and PCL-30B, respectively. The equilibrium melting temperatures of the nanocomposites decreased as a result of interaction between matrix and organoclays. The calculated values of χ's (using eq 1) are thus obtained as -4.91×10^{-5} and -9.95×10^{-5} for PCL-C18 and PCL-30B, respectively. The lower χ value for PCL-30B indicates stronger interaction between its components as compared to PCL-C18 nanocomposite. A similar value of χ (-8.0×10^{-5}) between PCL and other miscible polymer has been reported in the literature (49). The greater interaction in PCL-30B has also been observed in FTIR analyses with the shifting of

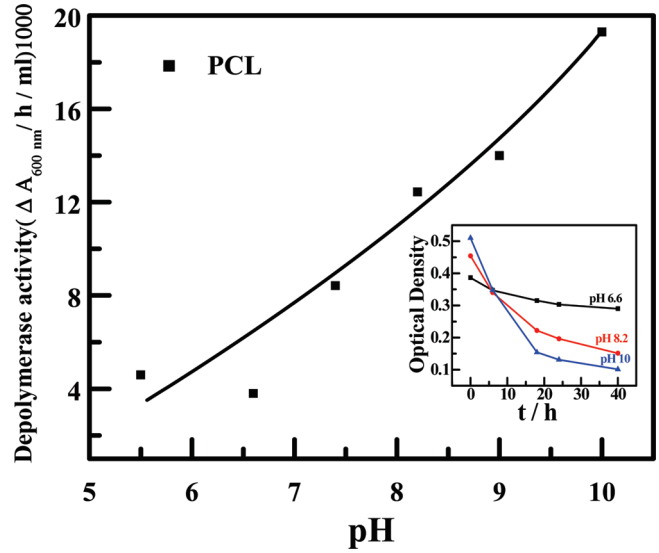

FIGURE 13. Effect of pH on *Aspergillus fumigatus* PCL–depolymerase activity. The inset figure represents the optical density of PCL suspension of varying pH as a function of time in hour. The depolymerase activity was calculated the initial slope of the curves.

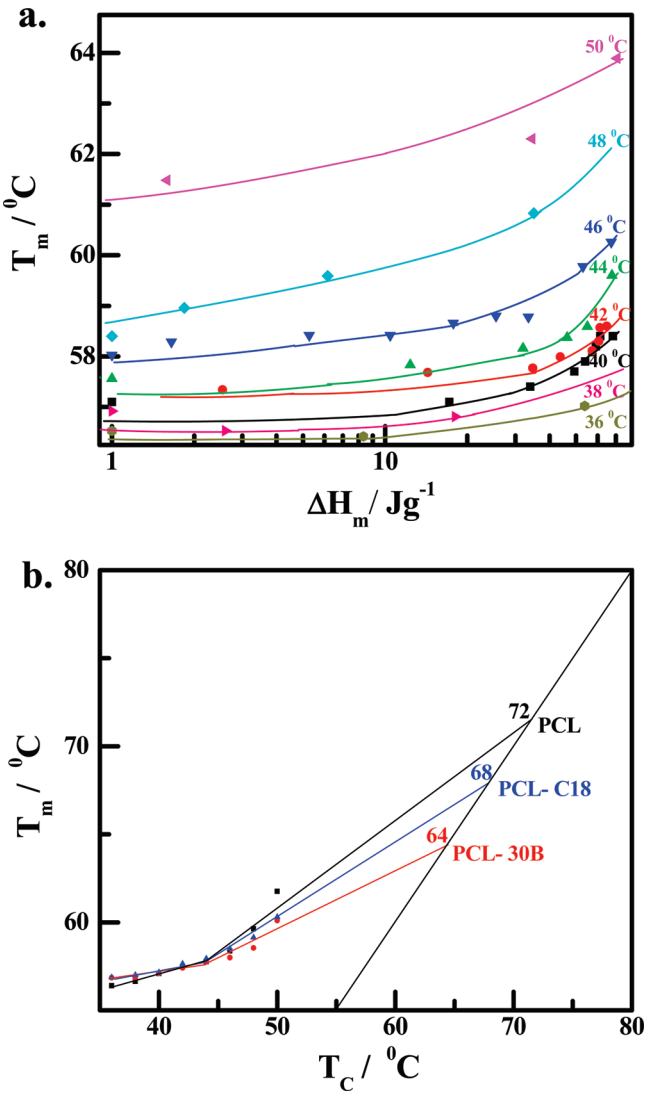

FIGURE 14. (a) Representative plot of melting temperatures (T_m) vs heat of fusion (ΔH) of pure PCL at the indicated crystallization temperatures (T_c). (b) $T_m - T_c$ plot at 5% ΔH for indicated specimens. The numbers show the corresponding equilibrium melting temperatures.

>C═O stretching frequency toward lower wavenumber (1727 cm^{-1}) with respect to pure PCL (1733 cm^{-1}) and PCL-C18 (1730 cm^{-1}) nanocomposites. The enhanced compatibility with 30B nanoclay arises from the specific interaction between the ester moiety of PCL and hydroxyethyl group of the organic modifier present in 30B through hydrogen bonding and can explain well why the crystallinity in PCL-30B is lower as compared to PCL-C18 (Table 1). On the other hand, the alkyl group present in C18 nanoclay can exert weak secondary interaction with PCL chains. This difference in interaction leads to the dissimilar property enhancement and nanostructure in two types of nanocomposites having different organic modifiers. The same idea of varying interactions, and thereby, the improved properties can be extended to other polymer−nanoclay systems of similar chemical in nature.

CONCLUSIONS

PCL/layered silicate nanocomposites have been prepared through solution route using two different types of organoclays. The nature of organic modifiers present in layered silicate markedly influences the properties of the nanocomposites. PCL forms intercalated nanostructure with C18 nanoclay, whereas it partially exfoliates 30B nanoclay and a disordered structure is evident both from XRD and TEM studies. Significant improvement in thermal and mechanical properties of the nanocomposites has been reported as compared to pristine PCL. Clay particles act as a nucleating agent for the crystallization of the matrix *PCL*. Biodegradation studies in enzyme, compost, and fungi media show remarkable enhancement of the biodegradation rate in nanocomposites in the presence of nanoclay as a result of varying crystallinity and depolymerase activity at different pH arising out of clay incorporation in the matrix. The absence of any biodegradation in distilled water and alkaline buffer solution confirms that the presence of microorganism is a precondition to initiate biodegradation of PCL. Finally, the rate of biodegradation can be fine-tuned either by the addition of nanoclays (to increase biodegradation rate) or other processing conditions that affect the crystallinity of the samples (to decrease biodegradation rate). The extent of biodegradation has been shown by using scanning confocal and electron microscope images. The degree of compatibility between matrix and different types of organoclays has been revealed through interaction parameter (χ) quantitatively, which is the main reason behind the dissimilar property enhancement including nanostructure among nanocomposites.

Acknowledgment. The authors acknowledge the receipt of research funding from Department of Biotechnology (DBT), New Delhi, Ministry of Science and Technology, Government of India (Project BT/PR-6929/BCE/08/433/2005). The national facility of Scanning Confocal Microscopy under Prof. S.C. Lakhotia, supported by DST, India, is also gratefully acknowledged.

Supporting Information Available: Additional information as noted in the text (PDF and AVI). This material is available free of charge via the Internet at http://pubs.acs.org.

REFERENCES AND NOTES

(1) Mayer, J. M.; Kaplan, D. L. *Trends Polym. Sci.* **1994**, *2*, 227.
(2) Kweon, H. Y.; Yoo, M. K.; Park, I. K.; Kim, T. H.; Lee, H. C.; et al. *Biomaterials* **2003**, *24*, 801.
(3) Giannelis, E. P. *Adv. Mater.* **1996**, *8*, 29–35.
(4) LeBaron, P. C.; Wang, Z.; Pinnavaia, T. J. *Appl. Clay Sci.* **1999**, *15*, 11.
(5) Vaia, R. A.; Ishii, H.; Giannelis, E. P. *Chem. Mater.* **1993**, *5*, 1694.
(6) Usuki, A.; Kojima, Y.; Kawasumi, M.; Okada, A.; Fukushima, Y.; Kurauchi, T.; Kamigaito, O. *J. Mater. Res.* **1993**, *8*, 1179–1184.
(7) Balsamo, V.; Calzadilla, N.; Mora, G.; Muller, A. J. *J. Polym. Sci., Part B: Polym Phys.* **2001**, *39*, 771.
(8) Ciardelli, G.; Chiono, V.; Vozzi, G.; Pracella, M.; Ahluwalia, A.; Barbani, N.; Cristallini, C.; Giusti, P. *Biomacromolecules* **2005**, *6*, 1961.
(9) Wu, C. S. *Polymer* **2005**, *46*, 147.
(10) Homminga, D.; Goderis, B.; Dolbnya, I.; Groeninckx, G. *Polymer* **2006**, *47*, 1620.
(11) Chen, E. C.; Wu, T. M. *Polym. Degrad. Stab.* **2007**, *92*, 1009.
(12) Lepoittevin, B.; Pantoustier, N.; Devalckenaere, M.; Alexandre, M.; Calberg, C.; et al. *Polymer* **2003**, *44*, 2033.
(13) Luduena, L. N.; Alvarez, V. A.; Vazquez, A. *Mater. Sci. Eng., A* **2007**, *460−461*, 121.

(14) Saeed, K.; Park, S. Y.; Lee, H. J.; Baek, J. B.; Huh, W. S. *Polymer* **2006**, *47*, 8019.
(15) Chen, B.; Evans, J. R. G. *Macromolecules* **2006**, *39*, 747.
(16) Chrissafis, K.; Antoniadis, G.; Paraskevopoulos, K. M.; Vassiliou, A.; Bikiaris, D. N. *Compos. Sci. Technol.* **2007**, *67*, 2165.
(17) Wu, Z.; Yin, J.; Yan, S.; Xie, Y.; Ma, J.; Chen, X. *Polymer* **2007**, *48*, 6439.
(18) Lepoittevin, B.; Devalckenaere, M.; Pantoustier, N.; Alexandre, M.; Kubies, D.; Calberg, C.; Jerome, R.; Dubois, P. *Polymer* **2002**, *43*, 4017.
(19) Gorrasi, G.; Tortora, M.; Vittoria, V.; Pollet, E.; Lepoittevin, B.; Alexandre, M.; Dubois, P. *Polymer* **2003**, *44*, 2271.
(20) Rosa, D. S.; Filho, R. P.; Chui, Q. S. H.; Calil, M. R.; Guedes, C. G. F. *Eur. Polym. J.* **2003**, *39*, 233.
(21) Kesel, C. D.; Wauven, C. V.; David, C. *Polym. Degrad. Stab.* **1997**, *55*, 107.
(22) Sanchez, J. G.; Tsuchii, A.; Tokiwa, Y. *Biotechnol. Lett.* **2000**, *22*, 849.
(23) Kim, D. Y.; Rhee, Y. H. *Appl. Microbiol. Biotechnol.* **2003**, *61*, 300.
(24) Murphy, C. A.; Samuel, J. A. C.; Huang, S. J.; Vinopal, R. T. *Appl. Environ. Microb.* **1996**, *62*, 456.
(25) Chen, D. R.; Bei, J. Z.; Wang, S. G. *Polym. Degrad. Stab.* **2000**, *67*, 455.
(26) Oda, Y.; Asari, H.; Urakami, T.; Tonomura, K. *J. Ferment. Bioeng.* **1995**, *3*, 265.
(27) Hirotsu, T.; Ketelaars, A. A. J.; Nakayama, K. *Polym. Degrad. Stab.* **2000**, *68*, 311.
(28) Sinha Ray, S.; Okamoto, M.; Yamada, K.; Ueda, K. *Nano Lett.* **2002**, *2*, 1093.
(29) Sinha Ray, S.; Yamada, K.; Okamoto, M.; Ueda, K. *Polymer* **2003**, *44*, 857.
(30) Maiti, P.; Batt, C. A.; Giannelis, E. P. *Polym. Mater. Sci. Eng.* **2003**, *88*, 58.
(31) Sinha Ray, S.; Yamada, K.; Ogami, A.; Okamoto, M.; Ueda, K. *Macromol. Rapid Commun.* **2002**, *23*, 943.
(32) Maiti, P.; Yamada, K.; Okamoto, M.; Ueda, K.; Okamoto, K. *Chem. Mater.* **2002**, *14*, 4654.
(33) Maiti, P.; Yadav, P. J. P. *J. Nanosci. Nanotechnol.* **2008**, *8*, 1858.
(34) Williams, M. L.; Landel, R. F.; Ferry, J. D. *J. Am. Chem. Soc.* **1955**, *77*, 3701.
(35) Krishnamoorti, R.; Giannelis, E. P. *Macromolecules* **1997**, *30*, 4097.
(36) Parulekar, Y.; Mohanty, A. K. *Green Chem.* **2006**, *8*, 206.
(37) Maiti, P.; Batt, C. A.; Giannelis, E. P. *Biomacromolecues* **2007**, *8*, 3393.
(38) Nishida, I. I.; Tokiwa, Y. *J. Environ. Polym. Degrad.* **1993**, *1*, 227.
(39) Benedict, C. V.; Cameron, J. A.; Huang, S. J. *J. Appl. Polym. Sci.* **1983**, *28*, 335.
(40) Benedict, C. V.; Cook, W. J.; Parrett, P.; Cameron, J. A.; Huang, S. J.; Bell, J. P. *J. Appl. Polym. Sci.* **1983**, *28*, 327–334.
(41) Kumagai, Y.; Kanesawa, Y.; Doi, Y. *Makromol. Chem.* **1992**, *193*, 53.
(42) Li, S.; McCarthy, S. *Macromolecules* **1999**, *32*, 4454.
(43) Koyama, N.; Doi, Y. *Macromolecules* **1997**, *30*, 826.
(44) MacDonald, R. T.; McCarthy, S. P.; Gross, R. A. *Macromolecules* **1996**, *29*, 7356.
(45) Iwata, T.; Doi, Y. *Polym. Int.* **2002**, *51*, 852.
(46) Iwata, T.; Doi, Y. *Macromolecules* **1998**, *31*, 2461.
(47) Nishi, T.; Wang, T. T. *Macromolecules* **1975**, *8*, 909.
(48) Maiti, P.; Nandi, A. K. *Macromolecules* **1995**, *28*, 8511. Maiti, P.; Chatterjee, J.; Rana, D.; Nandi, A. K. *Polymer* **1993**, *34*, 4273.
(49) Yam, W. Y.; Ismail, J.; Kammer, H. W.; Schmidt, H.; Kummerlowe, C. *Polymer* **1999**, *40*, 5545.

AM900584R